The Impact of Convection on ENSO: From a Delayed Oscillator to a Series of Events

RICHARD B. NEALE, JADWIGA H. RICHTER, AND MARKUS JOCHUM

National Center for Atmospheric Research, Boulder, Colorado

(Manuscript received 14 September 2007, in final form 14 April 2008)

ABSTRACT

The NCAR Community Climate System Model, version 3 (CCSM3) exhibits persistent errors in its simulation of the El Niño–Southern Oscillation (ENSO) mode of coupled variability. The amplitude of the oscillation is too strong, the dominant 2-yr period too regular, and the width of the sea surface temperature response in the Pacific too narrow, with positive anomalies extending too far into the western Pacific. Two changes in the parameterization of deep convection result in a significant improvement to many aspects of the ENSO simulation. The inclusion of convective momentum transport (CMT) and a dilution approximation for the calculation of convective available potential energy (CAPE) are used in development integrations, and a striking improvement in ENSO characteristics is seen. An increase in the periodicity of ENSO is achieved by a reduction in the strength of the existing "short-circuited" delayed-oscillator mode. The off-equatorial response is weaker and less tropically confined, largely as a result of the CMT and an associated redistribution of zonal momentum. The Pacific east–west structure is improved in response to the presence of convective dilution and cooling provided by increased surface fluxes. The initiation of El Niño events is fundamentally different. Enhanced intraseasonal surface stress variability leads to absolute surface westerlies and a cooling–warming dipole between the Philippine Sea and western Pacific. Lag-regression analysis shows that intraseasonal variability may play a significant role in event initiation and maintenance as opposed to being a benign response to increased SSTs. Recent observational evidence appears to support such a leading relationship.

1. Introduction

El Niño–Southern Oscillation (ENSO) is the dominant coupled mode of tropical variability on interannual time scales (Rasmusson and Carpenter 1982). Its representation in coupled climate models remains unsatisfactory (Achutarao and Sperber 2002, 2006) and the observed mechanisms by which it operates are somewhat unclear (Hendon et al. 2007). Prior to the large El Niño event of 1997–98 the number of proposed mechanisms was few. Research post-1997 firmly established the delayed oscillator (Suarez and Schopf 1988) and the recharge–discharge (Jin 1997) paradigms, as well as hybrid explanations (Picaut et al. 1997) and unified theories (Wang 2001). The exceptional El Niño event of 1997–98 was preceded by a number of westerly wind events (WWEs) in the western Pacific during the previous spring, attributed to the eastward propagating Madden–Julian oscillation (MJO) mode of intraseasonal variability (McPhaden 1999). This raised interest in the MJO–ENSO relationship considerably and numerous studies since have addressed the role of WWEs in initiating, maintaining, and modulating ENSO events (e.g., Hendon et al. 2007). Mechanistically, the preceding MJO episodes in 1997 appeared to generate a succession of downwelling Kelvin waves advecting warm western Pacific SSTs into the central Pacific and provided significant depressions in the 20°C isotherm across the entire Pacific basin (McPhaden and Yu 1999).

Coupled ocean–atmosphere modeling studies show that the growth trajectory of an individual El Niño event can be significantly strengthened by WWEs (Lengaigne et al. 2004). As appears to be the case with the observed 1997–98 El Niño, the modeled succession of events leading from WWEs to a mature El Niño involves SST warming in three phases (Zhang and Gottschalck 2002): First, the forced downwelling oceanic Kelvin wave in the western Pacific leads to local warming; then the central Pacific progression of the wave acts to advect and extend the warm pool into the

Corresponding author address: Richard Neale, National Center for Atmospheric Research, P.O. Box 3000, Boulder, CO 80307-3000.
E-mail: rneale@ucar.edu

DOI: 10.1175/2008JCLI2244.1

central Pacific; and, finally, the flattening of the basinwide SST gradient reduces the strength of the mean easterlies, leading to a basinwide instability. Once an El Niño is established, WWEs have also been shown to maintain the warm SST in the central Pacific, in a linear superposition sense, by further weakening the existing weak easterlies (Lengaigne et al. 2003; Zavala-Garay et al. 2005).

The predictability in the strength and duration of an individual El Niño is by no means certain with WWEs in place (Lengaigne et al. 2004) and a particular event may still manifest itself in the absence of significant stochastic forcing. This is supported by evidence that the observed system can be modeled as a stable linear system driven by integrated stochastic noise (Penland and Sardeshmukh 1995). Even prior to the 1997–98 El Niño the Pacific Ocean had built up a significant amount of heat before any MJO-related activity occurred (McPhaden 1999). This suggests that there is still a significant role for the ocean in setting the intrinsic ENSO frequency; however, observations point to an episodic as much as a cyclic phenomenon (Kessler 2002). The latitudinal width of the atmospheric trade wind response to SST anomalies associated with a particular event appears key to setting this intrinsic ENSO frequency. In a simple coupled model framework the generation of off-equatorial oceanic Rossby waves at the correct latitude (and therefore phase speed) is consistent with an atmospheric response of the correct width (Kirtman 1997). Coupled GCMs that simulate the ENSO frequency with too short a period, a common problem, tend to have an anomalous ENSO response that is too narrow in latitude (Capotondi et al. 2006; Davey et al. 2002). Recent modeling evidence suggests that including convective momentum transport (CMT) may improve this bias (Wittenberg et al. 2006).

If intraseasonal wind variance fidelity is, indeed, important for the evolution of ENSO, then improving the representation of atmospheric convective processes is paramount. Reinforcing this need is evidence showing the atmospheric model configuration as being the dominant source of ENSO simulation error in many current coupled model configurations (Guilyardi et al. 2004). At the time of the 1997–98 El Niño models had significant difficulty in representing the strength and phase of the MJO (Slingo et al. 1996). A recent review of modeling progress (Lin et al. 2006) concludes that problems still remain. The current incarnation of the Community Climate System Model, version 3 (CCSM3), (Collins et al. 2006b) lacks significant atmospheric intraseasonal variability and exhibits excessive Pacific trade winds in close proximity to the equator, both of which may in part explain its poor ENSO simulation.

Of focus in this study is the role that the Pacific latitudinal surface stress distribution and the atmospheric intraseasonal variability play in the triggering and modulation of ENSO events. We make two changes to the existing parameterization of deep convection (Zhang and McFarlane 1995, hereafter ZM95) and demonstrate significant improvements to both strength of intraseasonal variance and fidelity of the coupled simulation in CCSM3. We show that the two changes lead to significant improvements in the ENSO simulation, traceable to components that also form part of the observed ENSO: the oceanic delayed oscillator, convective suppression over cooler water, and WWE activity in the western Pacific.

Section 2 outlines the current CCSM3 configuration and the convection changes made in a development experiment. In section 3 the improvements to the model's mean simulation and the representation of ENSO are described, followed in section 4 by an investigation of the underlying changes to ENSO. Conclusions are presented in section 5.

2. Model description and experiments

The CCSM3 is a state-of-the-art climate simulation model consisting of atmosphere, ocean, land, and sea ice components in a fully coupled configuration. The atmosphere component is based largely on the Community Atmosphere Model, version 3 (CAM3; Collins et al. 2006a), with minor differences in the configuration. The coupled integrations (described here) use an atmosphere configured with a finite-volume dynamical core, 26 vertical levels, and a 1.9° latitude × 2.5° longitude horizontal grid. The ocean uses a nominal 1° horizontal grid with 40 levels in the vertical. Two fully coupled CCSM experiments were performed with development versions of the code. A 100-yr control experiment (C3OLD), closely resembling the climate simulated by CCSM3, and a 100-yr development experiment (C3NEW) with two changes to the ZM95 convection scheme are described below. The first 20 years were discarded to allow for tropical mixed layer depth equilibration and years 21–100 provided the main period of analysis. Years 81–100 provided the period of focus for the higher-frequency, daily output analysis.

a. A dilute plume approximation

The atmospheric deep convection parameterization in CCSM3 is a bulk mass flux approximation following ZM95. The closure in the scheme is provided by a rate limitation on the consumption of convective available potential energy (CAPE) over a predetermined time

scale (in this case, 1 h). The measure of CAPE used in the default version of CCSM3 uses a traditional definition, which we call "undilute" (UCAPE), defined as work that a parcel does on its environment as it ascends (with no mixing between the parcel and its environment) between a reference level and its level of neutral buoyancy. A typical conditionally unstable tropical ocean environment is able to maintain positive buoyancy, and convection frequently reaches the tropopause.

Essentially the scheme generates deep convection in the presence of UCAPE and the strength of the convective event is ultimately determined by the a priori UCAPE consumption time scale. This type of plume approximation is known to unrealistically bias the near-surface thermodynamic conditions and be relatively insensitive to the free-tropospheric humidity, particularly on subdiurnal time scales (Donner and Phillips 2003). An alternative method explored here allows mixing of the reference parcel with the free troposphere through mixing of entropy properties in a proportion depending on an assumed entrainment rate (Raymond and Blyth 1986, 1992). Such enhancement to the assumed mixing rate is both observationally more satisfying and potentially more likely to improve a model's intraseasonal variability (Lin et al. 2006).

b. Convective momentum transport

The standard version of CAM3 does not include convective momentum transport (CMT). In C3NEW we include the parameterization of CMT by deep convection based on the parameterization of Gregory et al. (1997). Following Kershaw and Gregory (1997) and based on the original theory of Schneider and Lindzen (1976) the effects of CMT in the CAM were examined in detail in Richter and Rasch (2008). They found that CMT improves several aspects of the CAM climate. In particular, CMT acts to reduce the equatorward flow in the lower winter branch of the Hadley circulation, reducing the CAM bias relative to observations. CMT reduces easterly bias in the tropics in the vicinity of the equator and the westerly bias in the Pacific north and south of the equator. As winds become more easterly in the equatorial central Pacific, the Walker circulation is strengthened and the precipitation increases in the western Pacific.

3. Model results

We show the impact of the changes to the convection here, with an attempt to sort out the mechanism for some of the changes in the following section.

a. Mean tropical climate

Figures 1a and 1b show the time-averaged model errors for precipitation. C3OLD exhibits a twin ITCZ, frequently found in coupled models in the Pacific (Lin 2007), with excessive precipitation errors (over 3 mm day^{-1}) centered at 15°N and 15°S. The Indian Ocean also has significant positive precipitation biases south of the equator, persistent throughout the year. Over Africa and Australia excessive precipitation dominates and erroneous monsoonal precipitation over Saudi Arabia is very apparent. In C3NEW the precipitation errors are significantly improved. The general shift of the precipitation maximum toward the western Pacific reduces the magnitude of the twin-ITCZ bias. Convective parcel dilution appears to reduce the excessive precipitation error over continental, seasonally dry regions. A noticeable degradation is the increase in precipitation over the northern Indian Ocean, owing to a slightly stronger Indian monsoon circulation.

Surface wind stress errors in C3OLD (Fig. 1c) are dominated by excessive oceanic trade winds, particularly along eastern basin regions. In addition, the equatorial central Pacific biases are a symptom of too weak mean easterlies. In C3NEW (Fig. 1d) the reduction of the twin-ITCZ precipitation bias and the redistribution of momentum by CMT lead to a significant reduction in the dominant trade wind and equatorial Pacific biases.

A concise assessment of tropical simulation fidelity appears in Fig. 2, using a Taylor diagram (Taylor 2001) over a 20-yr segment of each experiment. Marginal improvements are seen in the correlation pattern for well-simulated fields such as sea level pressure and temperature. Significant improvements (greater than 5%) are seen in the correlation patterns of both land and ocean precipitation. Most relevant to ENSO is the simulation of the equatorial zonal surface stress in the Pacific and, although this is the poorest simulated field (for both experiments), there is an 8% improvement in the correlation pattern and a reduction of the bias in C3NEW. The overall weighted RMSE for the analyzed variables has been reduced by about 10% in C3NEW compared to C3OLD, showing that there has been no degradation of the simulation in C3NEW.

b. ENSO simulation

Figure 3 characterizes SST variations in the Niño-3.4 region (5°N–5°S, 170°–120°W) for the model experiments and Hadley Centre Global Sea Ice and Sea Surface Temperature (HadISST) (Rayner et al. 2003) observations. C3OLD has a regular 2-yr period that is spectrally very distinct as shown by the dominant period in the wavelet analysis (Fig. 3a), fixed mostly at 2

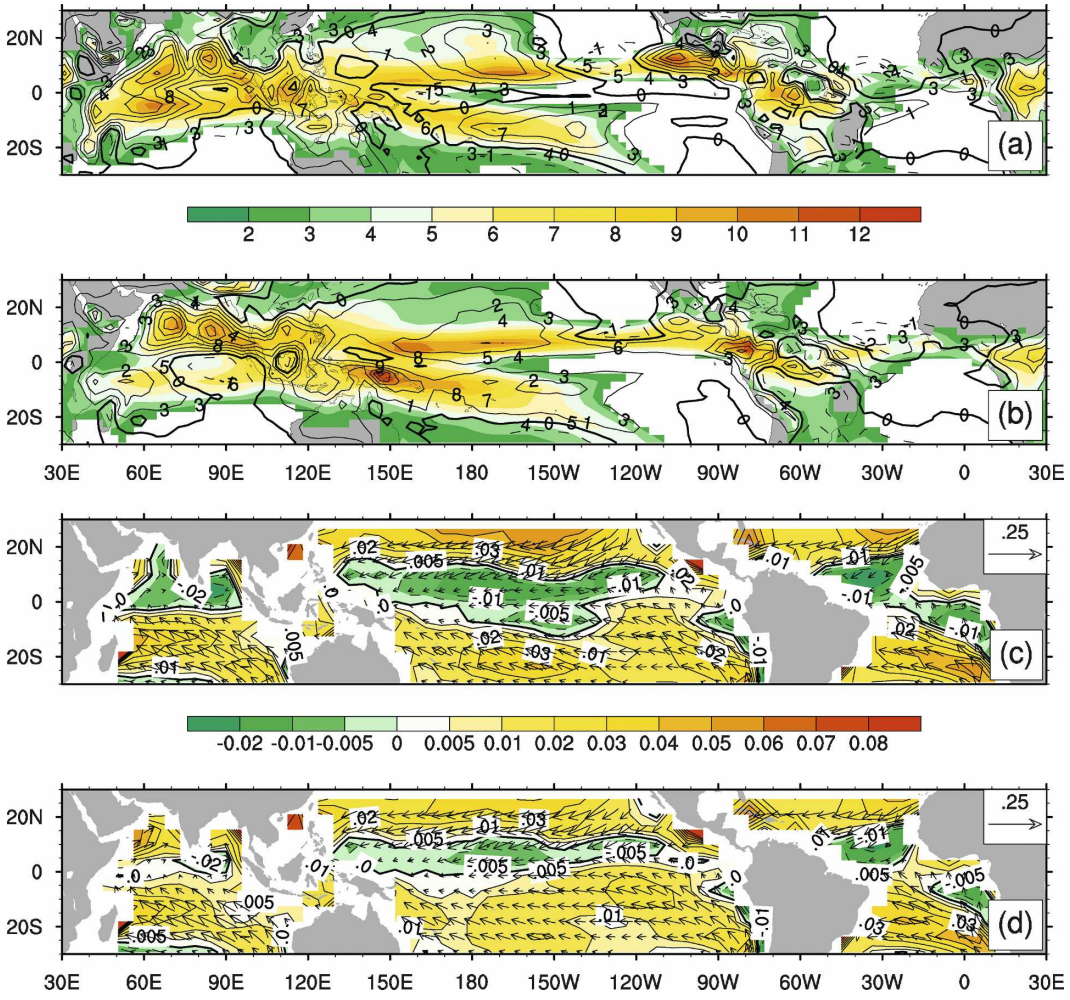

FIG. 1. Precipitation annual averages (mm day^{-1}, filled contours) and error [compared with the Global Precipitation Climatology Project (GPCP), line contours] for (a) C3OLD, (b) C3NEW, and surface stress annual averages (N m^{-2}, vectors) and error magnitude [compared with the European Remote Sensing Satellite (ERS), filled contours] for (c) C3OLD and (d) C3NEW.

yr and only briefly being 3 yr around year 50. This is consistent with the ENSO simulation from the release version of CCSM3 (Deser et al. 2006). C3NEW has a much-improved ENSO (Fig. 3b). The more realistic irregularity in the period is evident from both the SST anomaly time series and the wavelet analysis, in addition to the more realistic interdecadal variability in strength and period. Such variation reveals an ENSO more episodic than cyclic in nature, which may be more realistic (Kessler 2002). In the power spectra summary (Fig. 3d) it is clear that C3NEW has lower power and a broader spectral peak, similar to observations. A consequence of meandering in the dominant period is reflected in the autocorrelation characteristics (Fig. 3e). Successive events are much less predictable than in C3OLD. Not only is overall SST anomaly variance reduced, but it now peaks in the correct calendar month of November/December instead of August (Fig. 3f).

The geographical distribution of SST anomalies also shows clear improvement in C3NEW (Fig. 4). The observed pattern (Fig. 4a) shows a latitudinally broad, positive SST anomaly correlation across the central and east Pacific with weaker negative correlations in a typical horseshoe pattern from the subtropics through the tropical western Pacific. C3OLD (Fig. 4b) exhibits a much more zonal pattern with the positive correlation being confined to the deep tropics and then rapidly changing poleward to negative correlations across the western and central Pacific.

This narrow equatorial confinement tends to be seen in parallel with an unrealistic high ENSO frequency (Davey et al. 2002). Even in the east Pacific positive

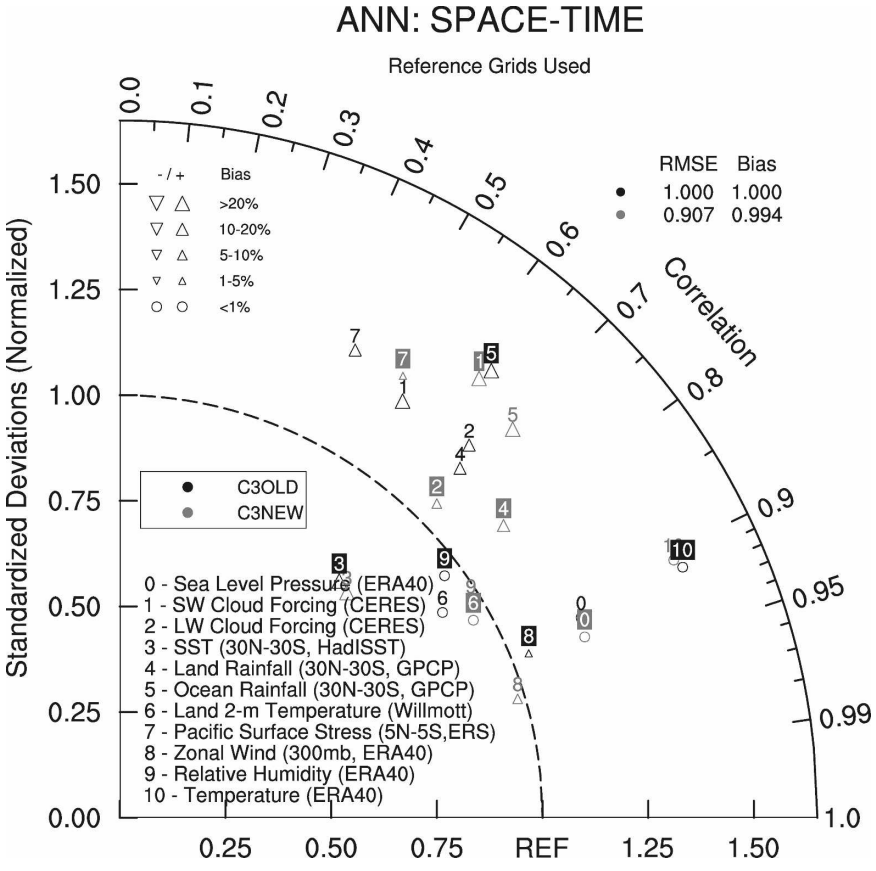

FIG. 2. Taylor diagram (Taylor 2001) showing the relative atmosphere improvements in the C3NEW experiment compared to C3OLD. Cosine of the angle represents the pattern correlation; azimuthal distance represents the standard deviation relative to observations. REF point represents zero RMSE compared to observations. For each individual point, upward (downward) pointing triangles represent a positive (negative) mean systematic bias. Solid filled squares are assigned to the experiment with the smallest absolute bias for each metric. The weighted RMSE and bias, relative to C3OLD, is shown in the top right. The domain of interest is global unless otherwise indicated.

correlations are too latitudinally confined and too large. C3NEW (Fig. 4c) more realistically reproduces the observations, particularly with a broader meridional structure and significant negative correlations in the western Pacific. However, the negative correlations extend too far west into the Indian Ocean, confining the positive SST anomaly teleconnection signal to the far west of that basin.

The improved seasonality in the C3NEW ENSO response is reflected in the evolution of a composite El Niño. Figure 5 shows the 2-yr evolution of a composite event (defined as the mean of the 13 strongest El Niño events from each experiment and as the mean of the 1982–83, 1986/87, 1991–92, 1994–95, and 1997–98 events for observations). The peak of the composite event occurs at JAN+ and is defined as the peak in observed Niño-3.4 SST anomalies. During JAN− through MAY−, prior to the peak of the composite El Niño, C3OLD (Fig. 5a) exhibits a strong transition from the previous La Niña, with SST anomalies increasing evenly across the entire Pacific basin. Precipitation anomalies also increase basinwide (Fig. 5b), particularly into JUL− when the Pacific SST reaches a seasonal maximum. During this time weak surface westerly anomalies in the central Pacific intensify and spread eastward (Fig. 5c). At least 3 months earlier than in observations AUG− sees the maximum in SST anomalies. SST anomalies then decrease, again basinwide, until a neutral ENSO phase is achieved in early FEB+. The anomalous precipitation increases again in concert with the second local maximum in the SST annual cycle in the central and eastern Pacific and then decreases rapidly with the transition to La Niña conditions. Anomalous surface westerlies (but still absolute

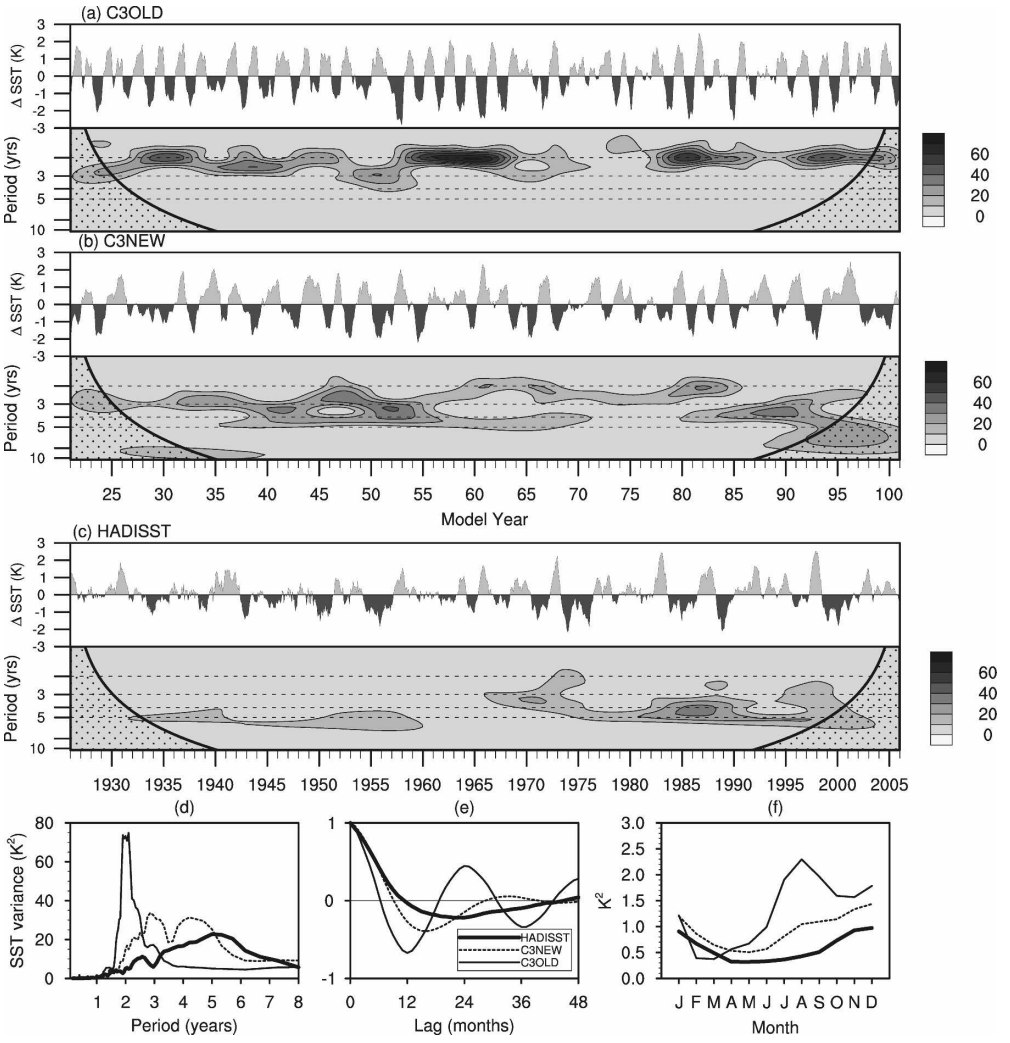

FIG. 3. Summary statistics of Niño-3.4 (5°N–5°S, 170°–120°W) monthly SST anomalies. Time series and wavelet analysis for model period years 21–100 for (a) C3OLD, (b) C3NEW, and (c) the most recent 80 years of the observed HadISST record in addition to (d) power spectra, (e) autocorrelation, and (f) average variance for each calendar month.

easterlies) are maintained at the same magnitude through DEC−, but there is a rapid switch to anomalous easterlies through the neutral phase of ENSO and into the subsequent La Niña. Consistent with the strong 2-yr periodicity a subsequent La Niña is almost fully established by NOV+.

C3NEW improves considerably upon the evolution seen in C3OLD. From JAN− onward there are significant, yet unsteady, surface westerly anomalies in the far western Pacific (Fig. 5f), in close agreement with the observations. These anomalies are a key to the different early evolution seen in C3OLD because they now lead to absolute westerlies through coherent intraseasonal convective events (discussed later). Concurrently there are weak positive SST and precipitation anomalies in the far western Pacific (Fig. 5d). During this period there is some evidence of eastward propagation of SST and zonal surface stress anomalies toward the central Pacific, even when viewed with monthly averaged data. This propagation is also very evident from the observed composite event and not dissimilar to the development of the 1997–98 El Niño in the northern spring of 2007 (McPhaden 1999).

From MAY− onward a basinwide response develops similar to C3OLD but with significant differences. Elevated central and east Pacific SST anomalies are accompanied by weak negative anomalies in the western Pacific. This is consistent with observations and with the negative SST anomaly correlations for C3NEW and HadISST, seen in Fig. 4. Accompanying the zonal di-

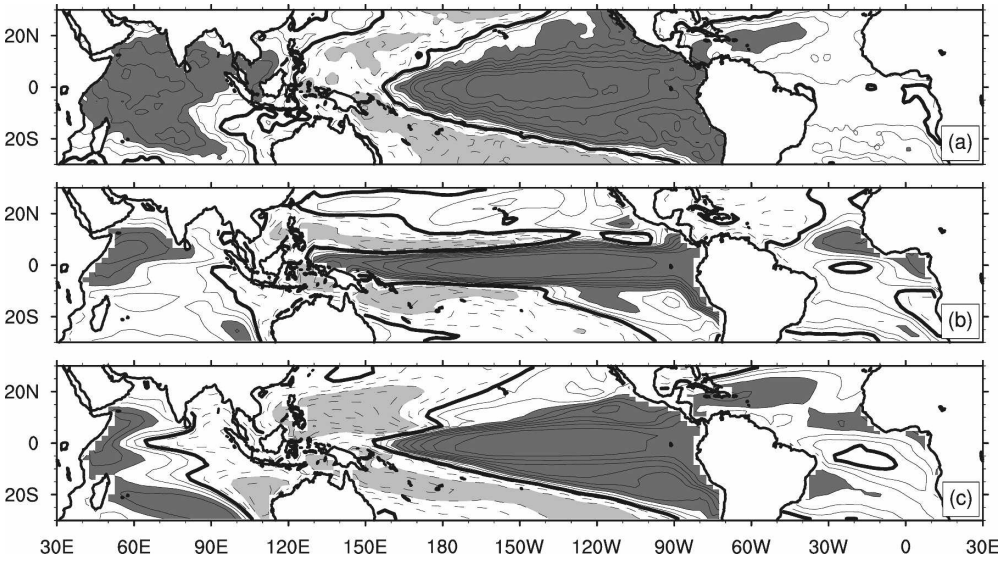

FIG. 4. Lag-zero correlation of Niño-3.4 and tropical SST anomalies for (a) HadISST, (b) C3OLD, and (c) C3NEW [contour interval is 0.1, and a correlation of >0.3 (filled contours) is significant at the 95% level for a conservative estimate of 40 degrees of freedom].

pole of SST anomalies is a similar dipole in precipitation anomalies with reduced precipitation in the western Pacific. This generates a much greater shift in the location of the precipitation maximum to the central Pacific compared to C3OLD. This reversal in the associated zonal gradient of atmospheric heating generates stronger westerly anomalies (which retain significant periods of absolute westelies) across the central and western Pacific. Unlike C3OLD, the El Niño SST anomalies reach a maximum in NOV−, around the same time as observed, and continue well into the following year. Strong anomalous easterlies develop in the far western Pacific through the first half of the following year, but the positive SSTs and precipitation anomalies are maintained well into MAY+. Weak surface easterlies then develop across the entire Pacific associated with a transition to neutral, then weak La Niña conditions.

4. ENSO mechanisms

Given that a significant improvement is seen in the ENSO simulation and the differences between the experiments are known (i.e., the addition of CMT and the switch to a dilute convective plume calculation), then it is pertinent to diagnose the reasons for the differences between the two ENSO simulations.

a. Atmospheric response

One of the most striking differences between the two experiments is the rapid and regular shift between successive El Niño and La Niña events in C3OLD. Figure 6 shows the evolution of SST anomalies for a composite El Niño. In the western Pacific Niño-4 region for C3OLD (Fig. 6a) positive SST anomalies develop in the deep tropics around APR− and grow to a maximum around SEP−. Only a couple of months after the onset of equatorial SST anomalies, negative anomalies develop off the equator at 5°–10°N and 5°–10°S. In C3NEW (Fig. 6c) the equatorial SST anomalies have a similar, if somewhat steadier, evolution, but off-equator development is absent until about SEP− and is located much farther poleward. The rapid transition to negative equatorial SST anomalies in C3OLD sees a similar off-equatorial response in opposite sign SST anomalies, indicating the rapid 2-yr period and a seemingly linear response to equatorial SST anomalies. C3NEW exhibits a much more gradual transition to La Niña conditions.

In the Niño-3 region of the central Pacific the SST anomalies develop a much more narrow response in C3OLD (Fig. 6b). At the time the C3NEW SST response starts expanding to about 15°N and 15°S (Fig. 6d), the C3OLD response is beginning to narrow and transition to a La Niña event. It is clear that the rapid transition of events in C3OLD is restricting the model's ability to fully develop a meridionally expansive response to the event.

Figure 7 reveals that there is a clear and rapid dynamical response to the Niño-4 increase in SSTs and associated tropospheric heating in C3OLD. The off-equatorial surface stress response is also strongly con-

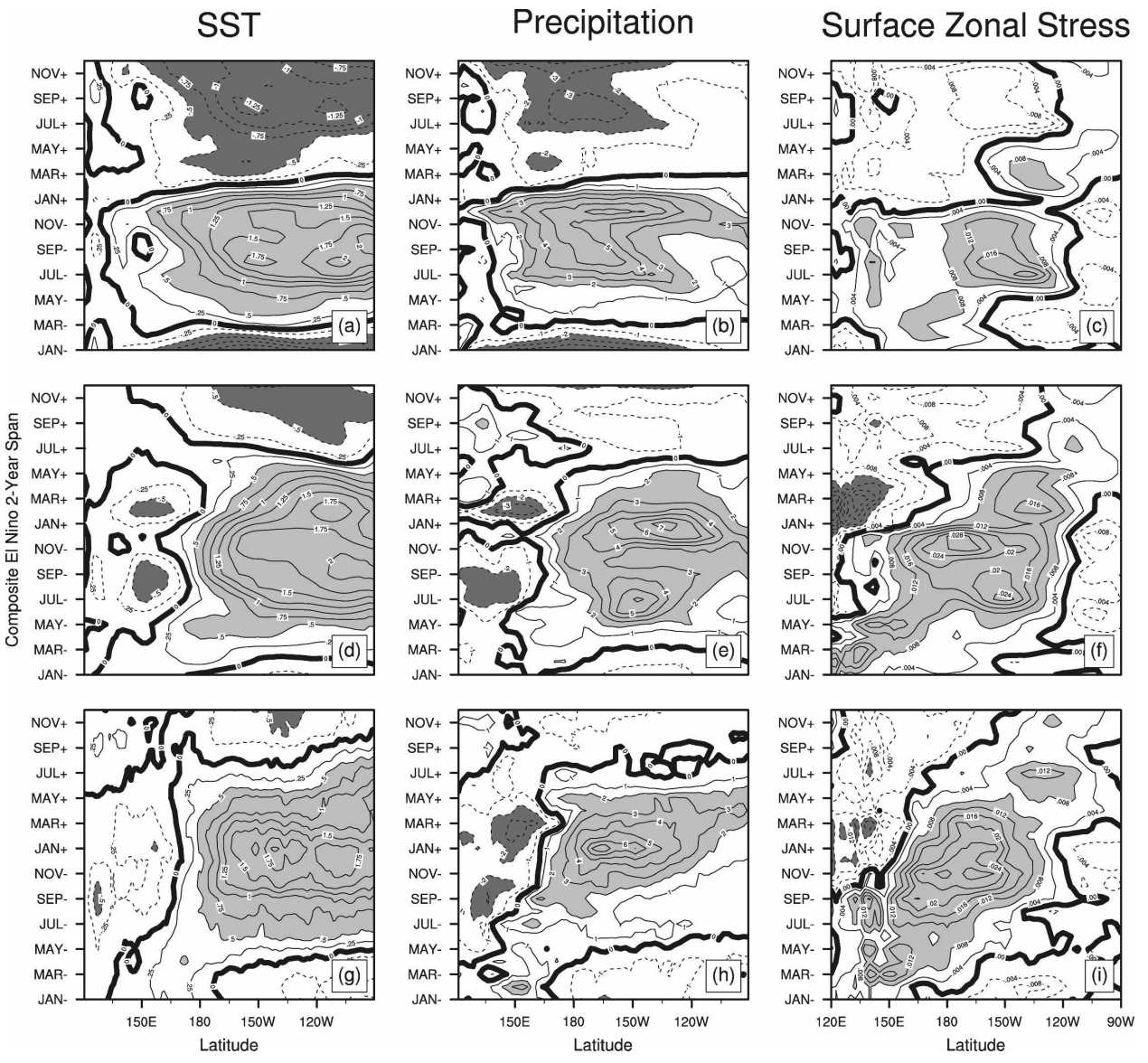

FIG. 5. Monthly anomalies from a 2-yr composite El Niño averaged between 5°N and 5°S for (top) C3OLD, (middle) C3NEW, and (bottom) observations (HadISST, GPCP, ERA-40) of (a), (d), (g) SST (K), (b), (e), (h) total precipitation, (mm day^{-1}), and (c), (f), (i) surface zonal stress (N m^{-2}).

fined latitudinally, consistent with the SST response in the previous figure. The equally strong response in meridional wind in the same region (Fig. 8a) suggests a strengthening in the local Hadley circulation in response to equatorial SST anomalies. These anomalies are somewhat invariant across the entire Pacific, leading to a locally enhanced ITCZ. In C3NEW the equatorial zonal stress anomalies respond to the stronger Niño-4 SST anomaly gradient (Fig. 7c) and clearly dominate over any response in the meridional sense (Fig. 8c). This is consistent with an anomalous Walker circulation observed during ENSO events and is responsible for the Southern Oscillation component of the phenomenon. Figure 9 clearly shows that the anomalous zonal Walker circulation is more dominant and realistic in C3NEW. In particular the low-level westerly anomalies are much stronger and deeper in the central and western Pacific. In the Niño-3 region the results show better agreement between the two experiments, suggesting that they are both responding to zonally oriented SST anomalies as expected (see Figs. 8b,d).

The model convection changes have a detectible role to play in the shift from a Hadley to a Walker type

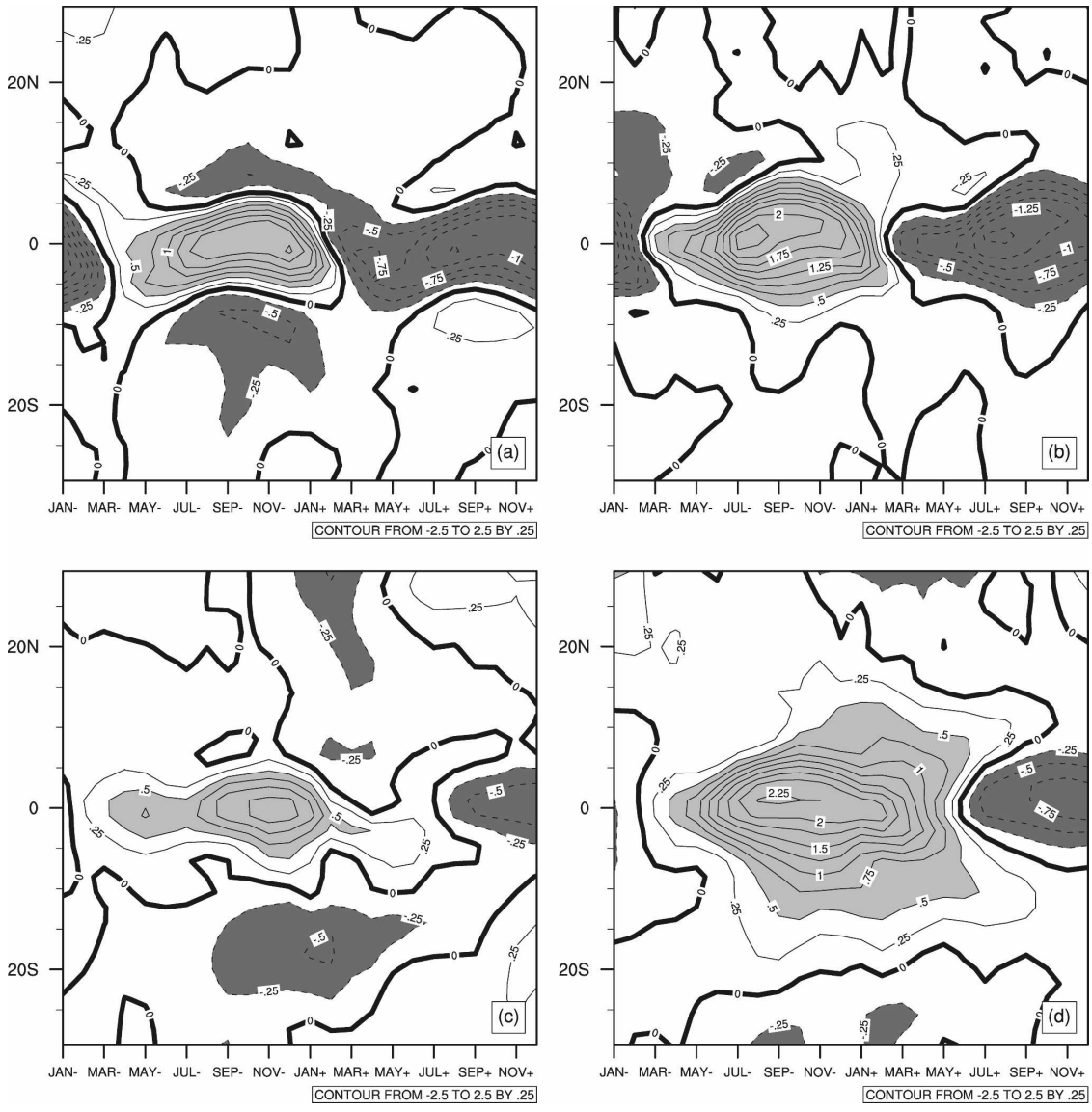

FIG. 6. SST anomalies (K) for a 2-yr composite El Niño period averaged over the Niño-4 region longitudes (160°E–150°W) for (a) C3OLD, and (c) C3NEW and over the Niño-3 region longitudes (150°–90°W) for (b) C3OLD and (d) C3NEW.

anomalous response. Richter and Rasch (2008) show that the mean effect of CMT is to reduce the strength of the Hadley circulation through the associated Coriolis torque. In C3NEW it appears that CMT is able to have a similar effect in both a mean and an anomalous sense. Figure 10 shows the mean and composite El Niño anomalies of zonal momentum tendency due to CMT, averaged for the Niño-4 region. The experiment used in this case is from a CAM-only, prescribed-SST simulation using the same atmosphere as in C3NEW. The mean picture (Fig. 10a) is complex in the western Pacific, but the general effect of including CMT is to spin down the local Hadley circulation and reduce the mean poleward gradient of the zonal wind, particularly north of the equator. Although the anomalous El Niño forcing that leads to the CMT zonal wind tendencies is different from the mean forcing, the net effect of CMT tendencies on the poleward gradient of near-surface zonal wind during a composite El Niño (Fig. 10b) is much the same—but over a more limited latitudinal range. Between 10°N and 10°S the poleward gradient is reduced. The poleward gradient of surface zonal wind has important implications for the generation of oceanic waves through wind stress curl forcing. Changes in the mean and anomalous forcing and their effects on ENSO in the ocean will be discussed in the next section.

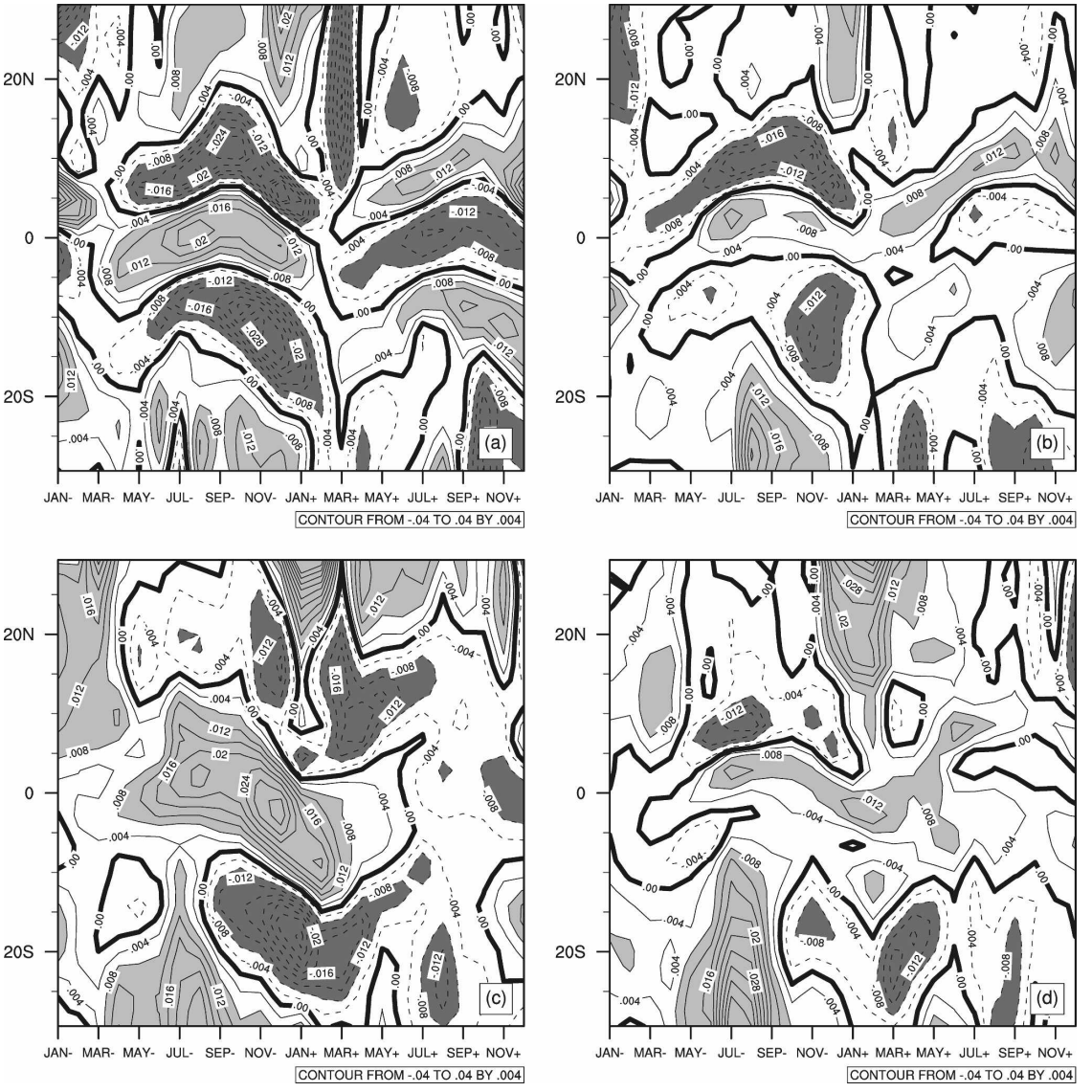

FIG. 7. As in Fig. 6 but for zonal surface stress (N m^{-2}).

b. Oceanic response

As discussed in the previous section, the improvements in reproducing ENSO are solely due to improvements in the representation of atmospheric convection. However, the memory of the system is often thought to lie in the planetary waves of the equatorial Pacific Ocean. Thus, planetary waves and their relation to wind stress anomalies is a convenient starting point to understand ENSO in CCSM.

Beginning with the early theories of Bjerknes (1969) and observations by Wyrtki (1975), it was established over the last three decades that El Niño is the result of a disturbance in the western Pacific warm pool that propagates eastward along the equatorial ocean where it creates a warm SST anomaly that subsequently leads to a breakdown of the Walker circulation [see Wang and Picault (2004) for a detailed description of ENSO theories]. The oceanic Kelvin wave that connects the western warm pool disturbance with the eastern SST anomaly is now well documented (e.g., McPhaden 1999), as is the fact that eastern Pacific warming is preceded by a discharge of warm water from the equator toward higher latitudes (Meinen and McPhaden 2000). A convenient way to illustrate the fundamental ocean processes involved in ENSO has been introduced by Kessler (2002) in a phase diagram that relates SST to thermocline depth (his Fig. 2). This figure has been reproduced here with the results from C3NEW to verify that C3NEW reproduces not only the observed

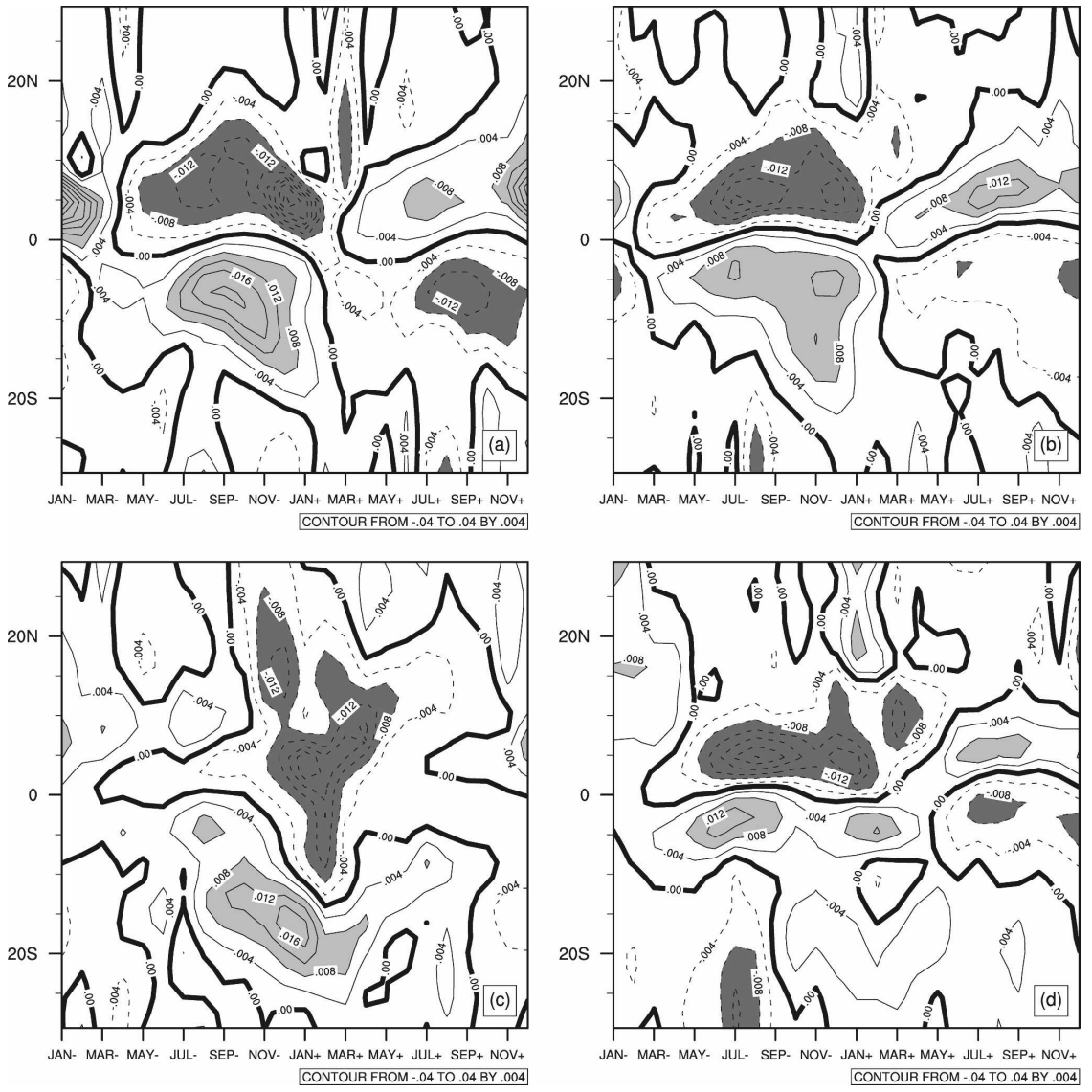

FIG. 8. As in Fig. 7 but for meridional surface stress.

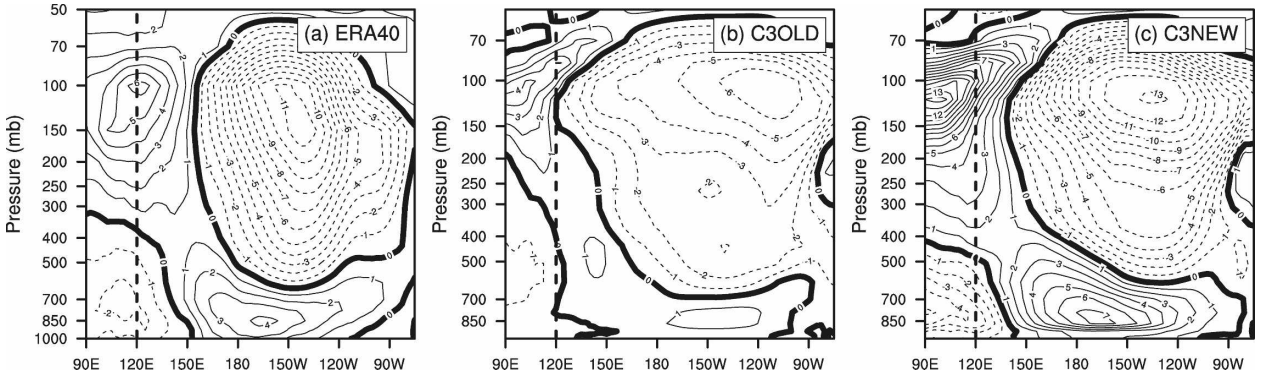

FIG. 9. Zonal wind (m s^{-1}), 5°N–5°S, for December–February (DJF) at the center of a 2-yr composite El Niño period for (a) ERA-40, (b) C3OLD, and (c) C3NEW. The vertical dashed line represents the approximate edge of the west Pacific.

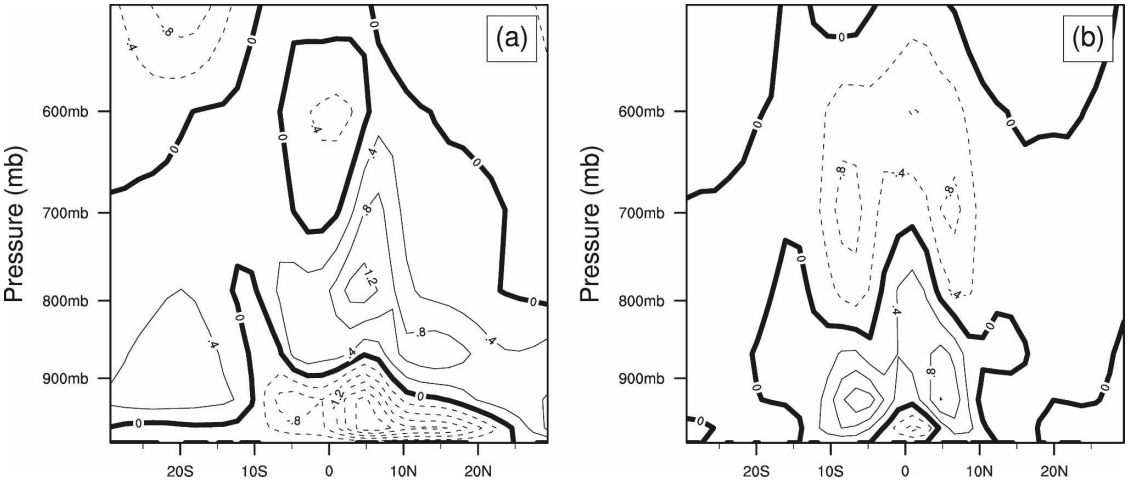

FIG. 10. Tendencies of zonal momentum ($m\,s^{-1}day^{-1}$) due to convective momentum transports averaged over the Niño-4 longitudes (160°E–150°W) from a prescribed SST experiment of C3NEW for (a) the DJF mean and (b) anomalies for the DJF peak of a 2-yr composite observed El Niño compared to the DJF mean in (a).

Niño-3 spectrum but also the underlying El Niño ocean dynamics (Fig. 11). Every point on that plot represents Niño-3 SST and the averaged depth of the 20°C isotherm at one particular month, and consecutive months are connected by a line; the strongest event in year 60 has been highlighted. The continuous light blue line illustrates the general phase space occupied by the system. Prior to a particular major event the system stays for 5 years in a neutral state (red line), recharges during weak La Niña conditions in the summer of year 59 (dark blue line), and then evolves into a strong El Niño that peaks in November year 60 (black line) [see Jin (1997) for a detailed description of the recharge/discharge concept]. While the system is rather uneventful during the first 5 yr, it takes only 15 months to cross the right-hand El Niño quadrants. The evolution of the

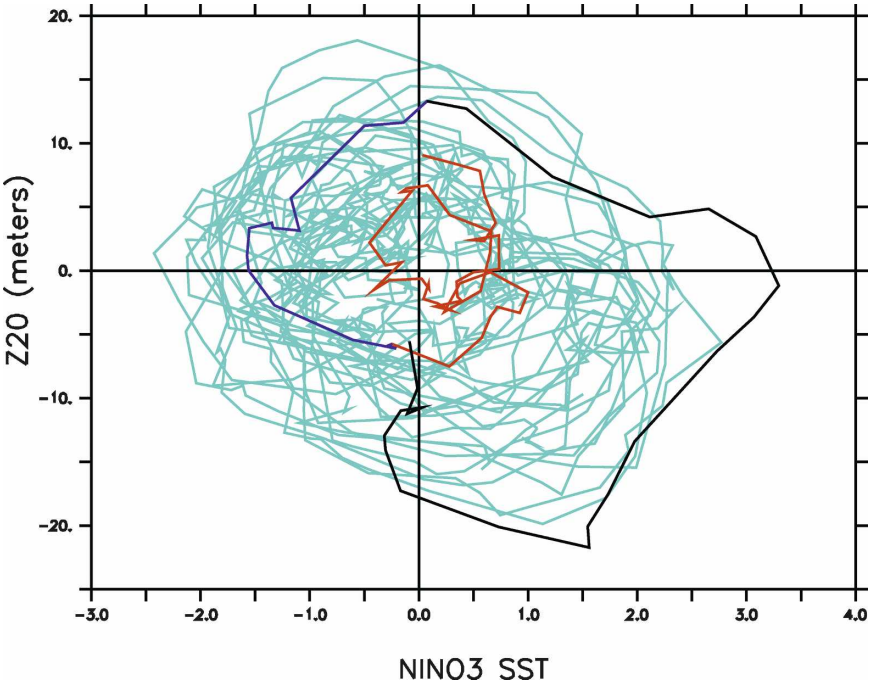

FIG. 11. Phase orbits of Niño-3 SST and zonal mean (5°S–5°N, 130°E–80°W) 20°C isotherm depth compared with the observations of Kessler (2002). See text for details.

1960–61 event is rather similar to the observed 1997–98 event, as described in Kessler (2002); for 6 years the equatorial Pacific stays close to the origin of the phase space, and then goes through a weak La Niña/recharge phase, which leads to an El Niño that peaks in November 1997. This observed event spent 17 months in the two right-hand quadrants, only a little longer than the 15 months it took in the model. Comparing the present, Fig. 11, one sees that the model also reproduces other important features of the observations: the thermocline depth varies between −25 and 20 m, Niño-3 SST varies between 2-K cold anomalies and 3-K warm anomalies, and the events are skewed so that there are relatively few large warming/discharge events and many small cooling/recharge events. As in the observations, the time lag between thermocline anomalies and subsequent Niño-3 anomalies is 9 months, with a correlation of 0.7 in the observations and 0.6 in the model. The Niño-3 spectrum of the previous section (Fig. 3) and the phase diagram in this section illustrate that C3NEW improves on the standard metrics that describe ENSO. We can now ask the question of what led to the significant improvement in the ENSO representation as compared to C3OLD?

The ENSO of C3OLD has been described in great detail by Deser et al. (2006), and we will describe here only the aspect that is relevant for understanding the dynamics. Figure 12 shows the correlation of the thermocline anomaly at 0°N, 120°W with the basinwide thermocline anomalies and the basinwide zonal wind stress anomalies at four different times (based on 80 years of model output). By construction, Fig. 12a shows the fully developed El Niño state: a deep thermocline anomaly in the east and a westerly wind stress anomaly to the west of it. Poleward of it there are easterly wind anomalies; both wind anomalies intensify for the next several months (Fig. 12b). There are two things worth noting: the easterly anomalies are too strong, compared to observations (see Deser et al. 2006, their Fig. 16), and the strong meridional shear in the wind stress creates upwelling Rossby waves at 5°S/N and downwelling Rossby waves at 10°S/N. In particular, note that these waves are created in the middle of the basin. Six months later the upwelling Rossby wave has reflected and terminates El Niño (Fig. 12c) and 14 months later the downwelling Rossby wave has set the stage for the next El Niño (Fig. 12d). Thus, in C3OLD the warm SST anomaly of El Niño creates zonal wind stress anomalies that lead to its termination as well as its recurrence. This atmospheric response in the central Pacific has already been described in ocean simulations forced with observed winds from an El Niño period (O'Brien et al. 1981). There, however, the resulting upwelling Kelvin wave was too weak to terminate El Niño. This is consistent with our assessment that the off-equatorial wind response to an equatorial warming of SST is too strong in C3OLD.

The analysis above suggests at least two changes to the CAM that could improve ENSO and bring the tropical surface winds more in accordance with observations: weaken the off-equatorial trade response, thereby reducing the off-equatorial wave response (Fig. 12b), and reverse the western warm pool response, thereby suppressing the terminating Kelvin wave (Fig. 12c). This was achieved by including the two changes to the convection parameterization described in the previous section, shown in Fig. 13. At first sight the El Niño development in C3NEW is rather similar to C3OLD; however, on closer inspection two major differences become apparent: after 4 months the off-equatorial trade response is much weaker and creates weaker upwelling and downwelling Rossby waves. In particular, the downwelling Rossby waves at 10°S/N are no longer created in the middle of the basin but are, indeed, the result of reflection at the eastern boundary (Fig. 13b). The second major change is that after 10 months the eastern part of the basin is dominated by a westerly wind anomaly that inhibits the propagation of the terminating Kelvin wave (Fig. 13c). Both changes act to weaken the deterministic structure of ENSO: in C3OLD the El Niño wind response immediately creates the terminating as well as the recurring Rossby wave that leads to a clockworklike succession of El Niño events. In C3NEW these mechanisms are still in place, but they are weakened and the outcome after 18 months is much less certain in C3NEW than in C3OLD, which, unlike C3NEW, already shows a clear El Niño signal after 18 months (Fig. 13d).

The Niño-3.4 SST spectrum, (Fig. 3) as well as the previous figure, shows that ENSO in C3NEW has lost its cyclical nature and is, hence, more realistic than in C3OLD (Kessler 2002). At least in the model context we can now investigate what triggers an El Niño event and what causes its demise. An analysis of the four strongest events in C3NEW shows that each event is associated with WWEs over the western warm pool. One particular event is shown in Fig. 14. Similar to the development of the 1997–98 ENSO (McPhaden 1999) there is a series of WWEs in the warm pool preceding El Niño; in June of model year 0095 this leads to an eastern thermocline anomaly that does not develop into an El Niño, but several months later a full El Niño finally develops. The connection between WWEs and El Niño is more clearly illustrated in Fig. 15, where the correlation analysis shows that the localized high-frequency WWEs are, indeed, followed by large-scale

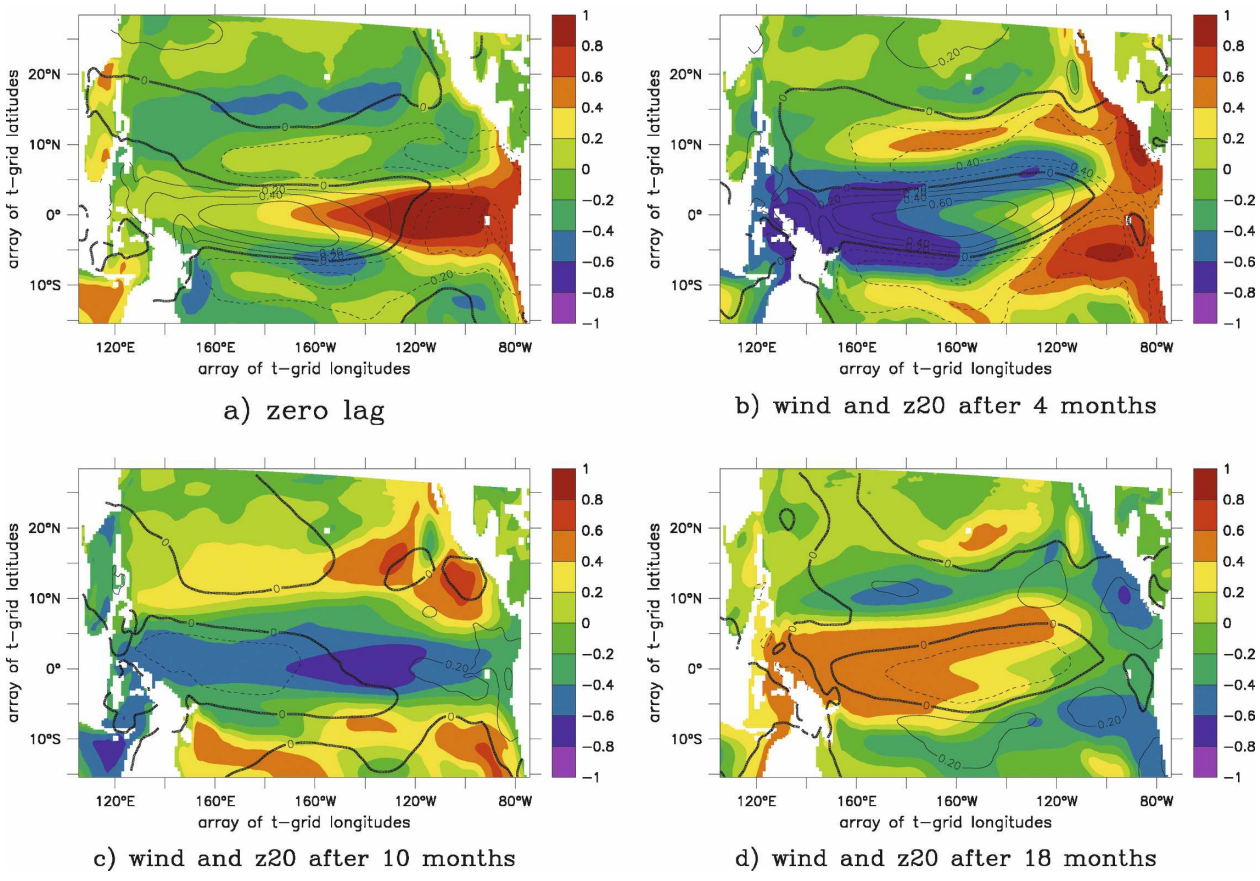

FIG. 12. Correlation of thermocline depth (Z_{20}) and zonal wind stress anomaly with the thermocline depth at 0°, 120°W in C3OLD.

thermocline anomalies. As in the observations, not all of the WWEs lead to an El Niño (Fig. 4) (Lengaigne et al. 2002), but WWEs clearly lead to downwelling Kelvin waves. Note that the WWEs in June 1995, December 1995, and June 1996 are all followed by upwelling Kelvin waves as well. On a larger scale this connection between an equatorial downwelling Kelvin wave and off-equatorial upwelling Rossby wave also happens in C3OLD; here it just happens on a smaller scale. Similar to the development of El Niño where it takes several downwelling waves to cause an event, the termination of El Niño also takes several upwelling Kelvin waves. Only the third finally succeeds in terminating El Niño in December 1996 because the prevailing westerly anomalies inhibit the propagation of the previous upwelling waves.

The discussion above highlights two things: first, compared to C3OLD, the atmospheric response to El Niño in C3NEW is weaker and also dampens the terminating Kelvin wave and, second, WWEs and anomalies are a central element of the ENSO in C3NEW. A dynamically important question is, then, whether the WWEs in C3NEW are causing El Niño or whether an extension of the warm pool causes increased activity and leads El Niño events. Observational evidence points in both directions: WWEs lead to an increased SST (Vecchi and Harrison 2000), and increased SST leads to increased WWE activity (Yu et al. 2003). The difficulties in analyzing the observations and establishing a clear cause–effect relationship point to a weak positive feedback between western warm pool SST and WWE activity (Eisenman et al. 2005; Hendon et al. 2007; Keen 1982). Note also that recent satellite observations show a positive correlation between SST and surface wind stress (Chelton et al. 2001; Hashizume et al. 2001). For the case of WWEs this indicates that the strength of WWEs may be independent of SST, but the ocean-relevant wind stress is not. As in the observations, it is not possible within the described experiment to clearly distinguish between cause and effect.

In summing up the ocean-based analysis provided thus far we conclude that ENSO in C3OLD is a self-sustained coupled ocean–atmosphere oscillation, whereas in C3NEW it is a damped and weaker oscillation that allows a larger role for atmospheric high frequency variability (WWEs). The structure of the WWEs is discussed in the following section.

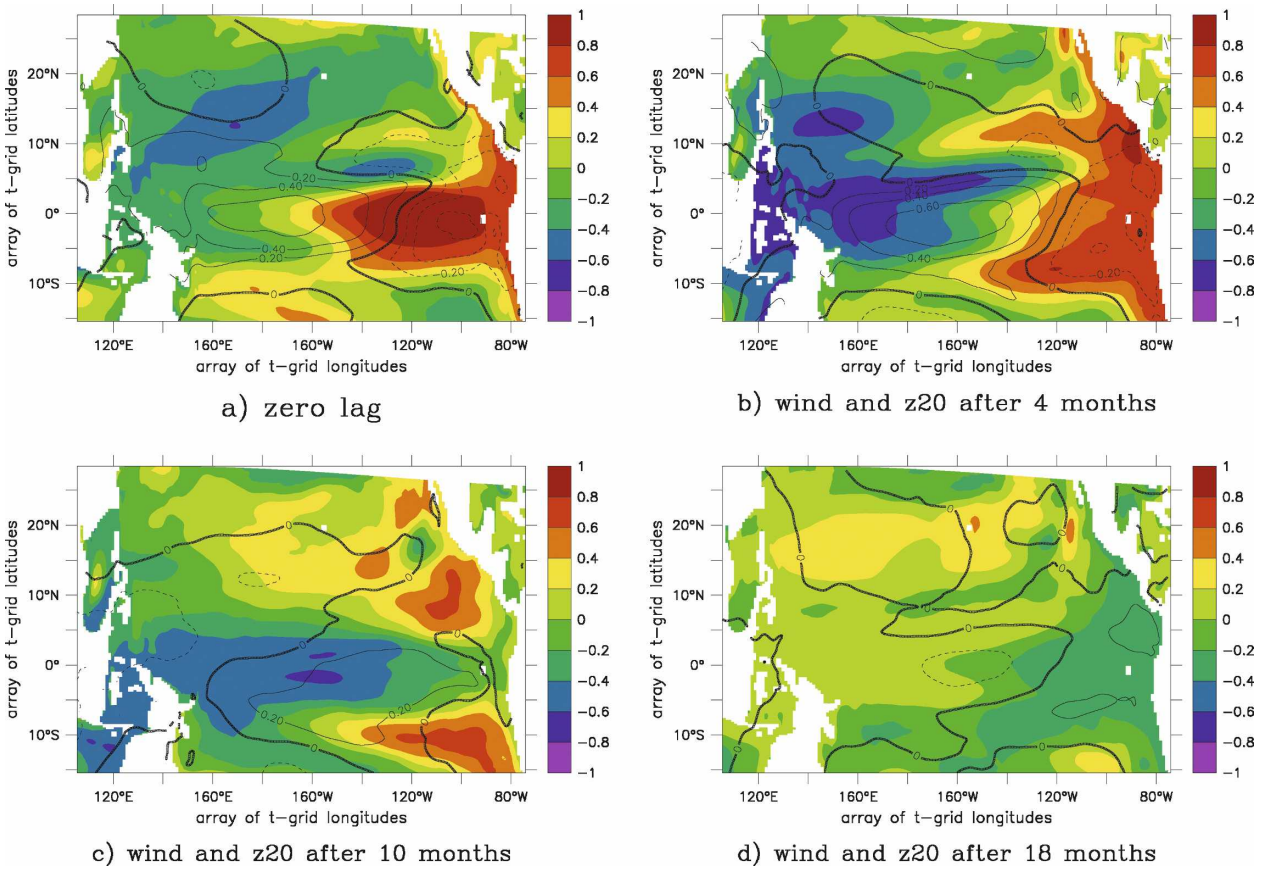

FIG. 13. As in Fig. 12 but for C3NEW.

c. *Westerly wind events and the MJO*

The questions we ask here are whether the modeled El Niño events are preceded and possibly initiated by WWEs and whether WWEs have any role in maintaining particular El Niño events. These are pertinent questions, given the implications for seasonal prediction.

The strongest observed WWEs are associated with MJO disturbances, which was also the case during the 1997–98 El Niño. Common with many climate models, CCSM3 underestimates intraseasonal variance associated with the MJO. Following Wheeler and Kiladis (1999), variance of the filtered MJO tropical wave signal (for zonal wavenumbers 1–5 and for periods 30–90 days) from tropical top-of-atmosphere outgoing longwave radiation (OLR) is shown in Fig. 16. Observations are from daily averaged NOAA OLR (Liebmann and Smith 1996). Variance in C3OLD during northern winter is less than 50% of the observed value and, although the maximum is approximately at the correct longitude, it is erroneously north rather than south of the equator. During northern summer, although there is a local maximum in the Indian Ocean, the maximum is again too weak and is now south of the equator, instead of north. In C3NEW there is a significant increase in the strength of MJO activity in boreal winter, particularly south of the equator in the western Pacific where the observed maximum is located between the Maritime Continent and Australia. The modeled maximum variance is now close to 80% of the observed value; however, there is still a local minimum on the equator that reflects the model's general inability to correctly simulate the strength of equatorial convection.

To investigate the relationship between MJO activity and ENSO an analysis following the methodology of Hendon et al. (2007) was performed. Daily values of anomalous OLR are filtered in wavenumber–frequency space in the same way as shown in Fig. 16 and averaged between 5°N and 5°S. Lag-correlations between a smoothed, 3-monthly running mean version of the square root of this time series and the January Niño-3.4 SST indices are then computed. This analysis is aimed at determining any significant lag–lead MJO relationship with the evolution of peak Niño-3.4 SST anomalies. The collection of panels in Fig. 17 is a near-reproduction of the figures in Hendon et al. (2007). For

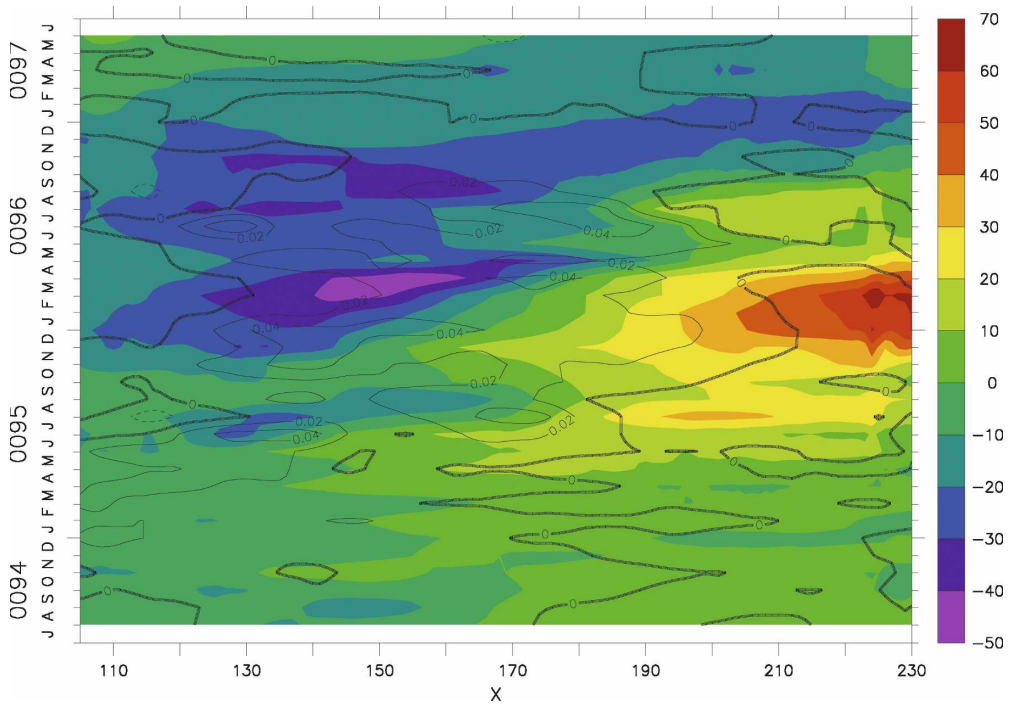

FIG. 14. Hovmoeller diagram of thermocline depth (color, m) and zonal wind stress anomaly (contour interval: 0.02 N m^{-2}) along the equator in C3NEW.

observed OLR (Fig. 17a) there is a significant relationship with MJO activity both during a peak in Niño-3.4 SST anomalies in the central Pacific and about 7 months prior to the Niño-3.4 SST anomaly peak centered on the western Pacific. With significant correlation values (greater than about 0.4) it provides evidence that increased MJO activity in the western Pacific many months prior to basinwide Pacific SST anomalies could be crucial for the initiation of ENSO events. The same analysis for 20 years of OLR for C3OLD and C3NEW (Figs. 17d,g) shows a significant relationship between peak Niño-3.4 SST anomalies and MJO activity in the central Pacific. In C3NEW, however, a stronger anomalous MJO increase is seen during the peak of ENSO events and extends further into the year following the Niño-3.4 SST peak. Neither experiment appears to have a strongly significant and coherent leading relationship.

A comparison of the same analysis for zonal surface stress appears to tell a somewhat different story. In observations (Fig. 17b) peak Niño-3.4 SST anomalies are accompanied by enhanced MJO surface stress anomalies in the central Pacific and reduced anomalies over the Maritime Continent. Any similar relationship appears weak in C3OLD (Fig. 17e), but in C3NEW (Fig. 17f) there is a significant increase in MJO-related surface stress anomalies across the entire Pacific. The anomalies continue well into the following year also. This much stronger dynamical signal of the MJO–ENSO relationship indicates that it is the absolute surface westerlies associated with a stronger MJO that are providing a two-way coupling between the developing El Niño and the enhanced MJO activity. Although this relationship appears weaker in observations, in C3NEW it is able, at times, to dominate the weaker oceanic delayed oscillator forcing. This retains warm SSTs over the entire Pacific basin and prevents the system from rapidly returning to a La Niña–like state.

There are also significant leading covariance and correlation patterns about 7 months prior to peak Niño-3.4 SST anomalies in the far western Pacific. This suggests that the dynamical part of the MJO may have a role in preconditioning the ocean prior to the full El Niño development. In the observations there is a suggestion that leading enhanced surface latent heating may result in a reduction in far western Pacific SSTs (Fig. 17c, McPhaden and Yu 1999), but for C3NEW a similar relationship remains inconclusive at the same lead time (Fig. 17i). A significant deficiency of the MJO–ENSO relationship that remains is the lack of negative correlation and covariance in the western Pacific at the time of peak Niño-3.4 SST. This may be a consequence of cold SST anomalies not being large enough to significantly reduce surface latent heat flux during MJO

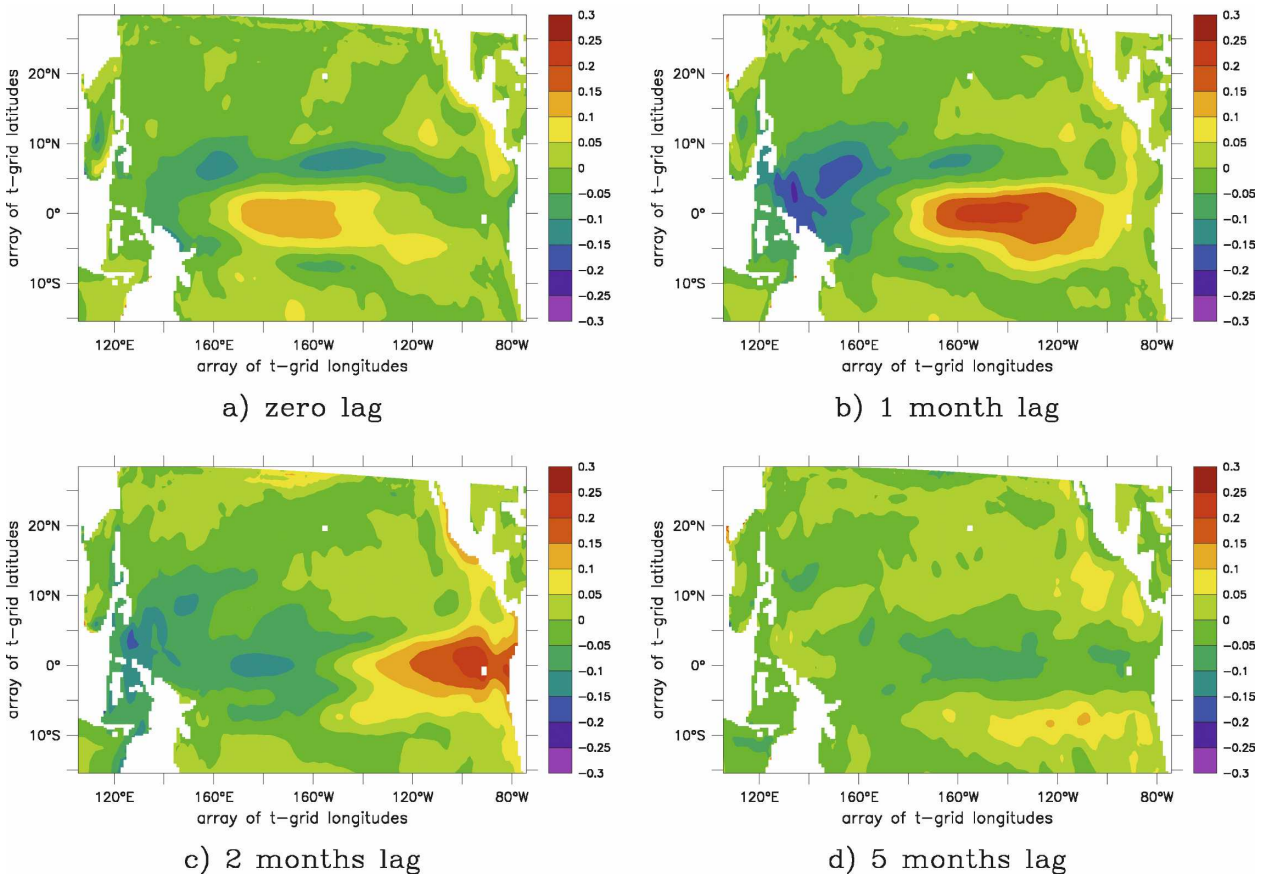

FIG. 15. Correlation of high-pass-filtered wind stress anomaly at 0°N, 170°E with thermocline depth anomalies based on 80 years of C3NEW.

events or deficiencies in the surface latent heat exchange during this time. Of course it may also be that MJO events are simply still not strong enough in C3NEW to generate a significant coupled relationship with seasonal SST variability.

5. Conclusions

It is illustrated here that by modifying the convection scheme in CCSM3, the ENSO regime shifts from a delayed oscillator to a series of events. The two responsible changes were both necessary, but not sufficient by themselves. Including convective momentum transport in the convection parameterization weakened the trades and the off-equatorial wind response to an El Niño event; allowing for convective plume entrainment strengthened MJO activity. The first process weakened the delayed oscillator, which produces the overly regular ENSO in C3OLD; the second process then added a mechanism for maintaining El Niño events. Whereas the plume entrainment leverages a more certain observed sensitivity of convection to humidity (Sherwood 1999), the uncertain effect of convective momentum transport continues to be incorporated in GCMs in a very simple way (e.g., Kim et al. 2008; Richter and Rasch 2008; Song et al. 2008; Wittenberg et al. 2006), mostly because of theoretical and observational uncertainties. It is possible that processes other than the ones described here appear to play a role but, since we are able to explain ENSO in C3OLD and C3NEW purely in the framework of a short-circuited delayed oscillator and as a series of events, we believe that they are secondary.

Not being able to reproduce ENSO properly always casts doubt on the quality of CCSM3 as a climate model, and the main purpose of the present study is to document for the CCSM3 user community the improvements in ENSO variability and how they were achieved. However, in illustrating the connections between changes in the convection scheme and ENSO, we believe that we also make a scientific contribution by adding to the increasing amount of evidence that shows

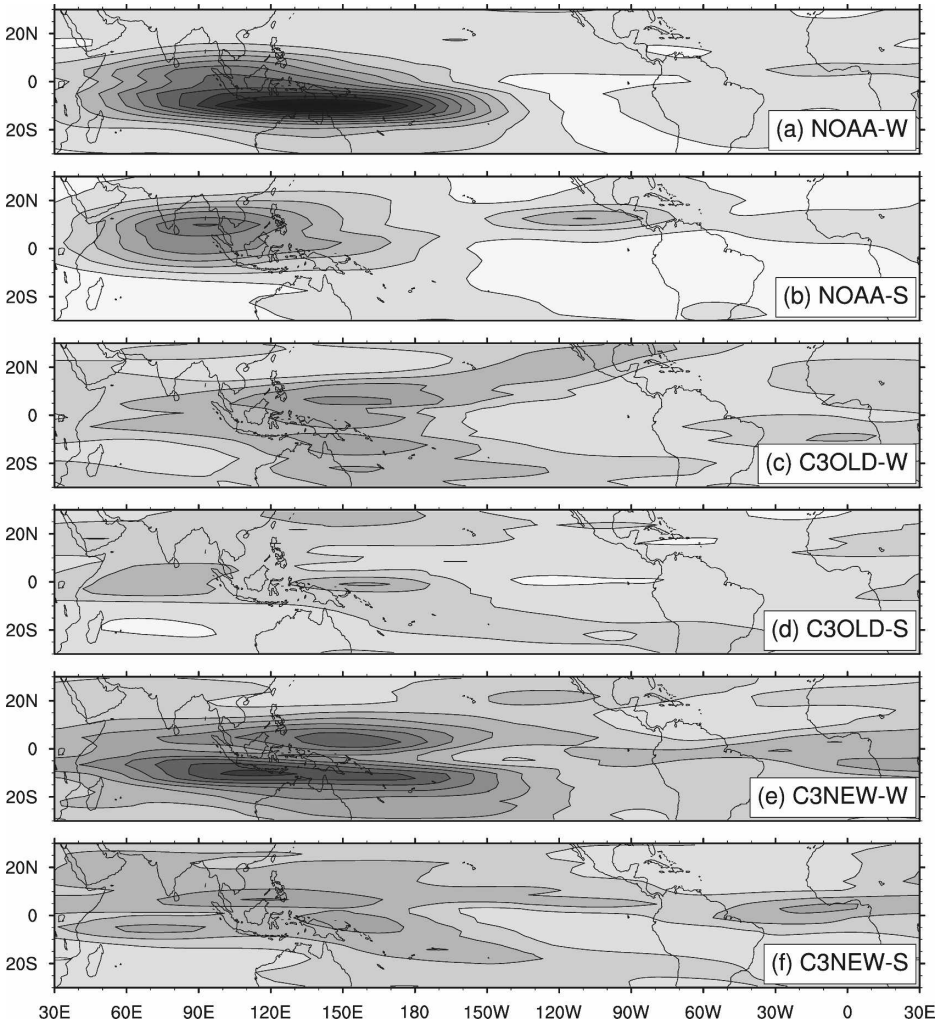

FIG. 16. Variance of outgoing longwave radiation for the MJO tropical wave mode of variability as filtered from a wavenumber–frequency analysis (see text) for (a), (b) NOAA interpolated OLR (1980–2000), (c), (d) C3NEW, and (e), (f) C3OLD during (a), (c), (e) winter and (b), (d), (f) summer. Contour interval is 20 $(\mathrm{W\ m^{-2}})^2$.

that ENSO is better described as a series of events, rather than an oscillation. The boundaries of course are blurred, because both C3OLD and C3NEW have stochastic as well oscillatory components; it is just that the relative impact of these components shifted. Comparison with the observations suggests that to explain the last 50 years of ENSO the stochastic component is more relevant, but this could be different in the past or future. Thus, future work will have to assess how sensitive off-equatorial air–sea coupling and MJO activity is to changes in the background state (e.g., warmer mean SST or stronger mean winds). It is worth noting, though, that the properties of ENSO in C3NEW are rather robust: they barely change during the course of our normal model development (e.g., changed hydrological cycle in the land model, changed parameterizations for subgrid ocean processes, and new sea ice model).

There are several important topics that are beyond the scope of the present study: the termination of El Niño, the generation of WWEs, and the biases in the mean and seasonal cycle. Regarding the termination of El Niño, we showed that in C3OLD it is terminated by an oceanic Kelvin wave that had its origin in the off-equatorial wind response to El Niño. In C3NEW this process became irrelevant, but we have yet to investigate what replaces it. We speculate that the realistic seasonality and length of El Niño events in C3NEW indicate that the seasonal changes in the eastern Pacific winds cause the termination as in the observations (Harrison and Vecchi 1999; Vecchi 2006), but this still requires more detailed study. For the WWEs we

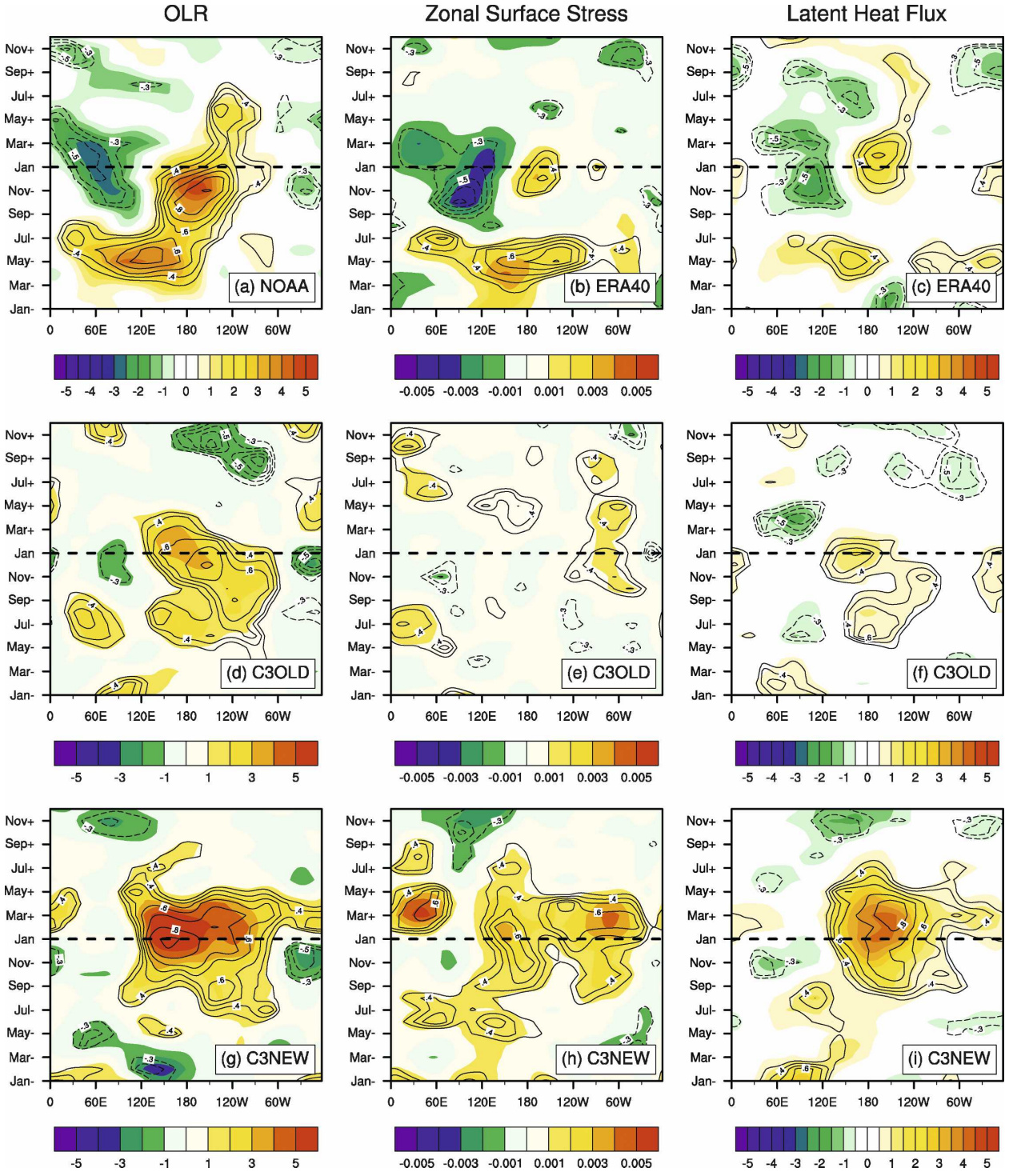

FIG. 17. Lag-regression (filled contours) and lag-correlation (line contours) of (left) MJO-filtered OLR (W m^{-2}), (middle) zonal surface stress (N m^{-2}), and (right) surface latent heat flux (W m^{-2}) against 3-month running mean January Niño-3.4 SST anomalies. Anomalies are scaled for a two standard anomaly of January Niño-3.4 SST.

showed that in C3NEW the statistics of their surface properties more closely resemble observations. Last, it should be pointed out that the changes in the convection schemes in C3NEW provided only marginal improvements to the precipitation biases in C3OLD, especially the "double ITCZ" in the eastern Pacific, which still remains. This suggests that the tropical eastern Pacific is merely reacting to events that are triggered in the western warm pool; it has no active part in the development of El Niño. This is also supported by a recent study of Jochum et al. (2008), which shows that removing the cold bias in the equatorial cold tongue (by allowing for tropical instability waves) has no impact on ENSO or the double ITCZ. It appears that ENSO and climate in the tropical eastern Pacific are controlled by two different regimes, with the former occasionally disrupting the latter.

Acknowledgments. The authors would like to acknowledge the substantial contribution to the CCSM project from the National Science Foundation (NSF), Department of Energy (DOE), the National Oceanic and Atmospheric Administration (NOAA), and the National Aeronautics and Space Administration (NASA). This study is based on model integrations performed at NCAR and the Oak Ridge National Laboratory (ORNL).

REFERENCES

Achutarao, K., and K. R. Sperber, 2002: Simulation of the El Niño Southern Oscillation: Results from the Coupled Model Intercomparison Project. *Climate Dyn.,* **19,** 191–209.

——, and ——, 2006: ENSO simulation in coupled ocean-atmosphere models: Are the current models better? *Climate Dyn.,* **27,** 1–15.

Bjerknes, J., 1969: Atmospheric teleconnections from the equatorial Pacific. *Mon. Wea. Rev.,* **97,** 163–172.

Capotondi, A., A. Wittenberg, and S. Masina, 2006: Spatial and temporal structure of tropical Pacific interannual variability in 20th century coupled simulations. *Ocean Modell.,* **15,** 274–298.

Chelton, D. B., and Coauthors, 2001: Observations of coupling between surface wind stress and sea surface temperature in the eastern tropical Pacific. *J. Climate,* **14,** 1479–1498.

Collins, W. D., and Coauthors, 2006a: The formulation and atmospheric simulation of the Community Atmosphere Model Version 3 (CAM3). *J. Climate,* **19,** 2144–2161.

——, and Coauthors, 2006b: The Community Climate System Model Version 3 (CCSM3). *J. Climate,* **19,** 2122–2143.

Davey, M. K., and Coauthors, 2002: STOIC: A study of coupled model climatology and variability in tropical ocean regions. *Climate Dyn.,* **18,** 403–420.

Deser, C., A. Capotondi, R. Saravanan, and A. Phillips, 2006: Tropical Pacific and Atlantic climate variability in CCSM3. *J. Climate,* **19,** 2451–2481.

Donner, L. J., and V. T. Phillips, 2003: Boundary layer control on convective available potential energy: Implications for cumulus parameterization. *J. Geophys. Res.,* **108,** 4701, doi:10.1029/2003JD003773.

Eisenman, I., L. Yu, and E. Tziperman, 2005: Westerly wind bursts: ENSO's tail rather than the dog? *J. Climate,* **18,** 5224–5237.

Gregory, D. R., R. Kershaw, and P. M. Inness, 1997: Parameterization of momentum transport by convection II: Tests in single-column and general circulation models. *Quart. J. Roy. Meteor. Soc.,* **123,** 1153–1183.

Guilyardi, E., and Coauthors, 2004: Representing El Niño in coupled ocean–atmosphere GCMs: The dominant role of the atmospheric component. *J. Climate,* **17,** 4623–4629.

Harrison, D. E., and G. A. Vecchi, 1999: On the termination of El Niño. *Geophys. Res. Lett.,* **26,** 1593–1596.

Hashizume, H., S. Xie, T. Liu, and K. Takeuchi, 2001: Local and remote atmospheric response due to tropical instability waves: A global view from space. *J. Geophys. Res.,* **106,** 10 173–10 185.

Hendon, H. H., M. C. Wheeler, and C. Zhang, 2007: Seasonal dependence of the MJO–ENSO relationship. *J. Climate,* **20,** 531–543.

Jin, F. F., 1997: An equatorial ocean recharge paradigm for ENSO. Part I: Conceptual model. *J. Atmos. Sci.,* **54,** 811–829.

Jochum, M., G. Danabasoglu, M. Holland, Y.-O. Kwon, and W. G. Large, 2008: Ocean viscosity and climate. *J. Geophys. Res.,* **113,** C06017, doi:10.1029/2007JC004515.

Keen, R. A., 1982: The role of cross-equatorial cyclone pairs in the Southern Oscillation. *Mon. Wea. Rev.,* **110,** 1405–1416.

Kershaw, R., and D. Gregory, 1997: Parameterization of momentum transport by convection. I: Theory and cloud modelling results. *Quart. J. Roy. Meteor. Soc.,* **123,** 1133–1151.

Kessler, W. S., 2002: Is ENSO a cycle or a series of events? *Geophys. Res. Lett.,* **29,** 2125, doi:10.1029/2002GL015924.

Kim, D., J.-S. Kug, I.-S. Kang, F.-F. Jin, and A. T. Wittenberg, 2008: Tropical Pacific impacts of convective momentum transport in the SNU coupled GCM. *Climate Dyn.*, **31** (2–3), 213–226.

Kirtman, B. P., 1997: Oceanic Rossby wave dynamics and the ENSO period in a coupled model. *J. Climate,* **10,** 1690–1704.

Lengaigne, M., J.-P. Boulanger, C. Menkes, S. Masson, G. Madec, and P. Delacluse, 2002: Ocean response to the March 1997 Westerly Wind Event. *J. Geophys. Res.,* **107,** 8015, doi:10.1029/2001JC000841.

——, ——, ——, G. Madec, and P. Delecluse, 2003: The March 1997 Westerly Wind Event and the onset of the 1997–98 El Niño: Understanding the role of the atmospheric response. *J. Climate,* **16,** 3330–3343.

——, E. Guilyardi, J.-P. Boulanger, C. Mankes, P. Delecluse, P. Inness, J. Cole, and J. Slingo, 2004: Triggering of El Niño by westerly wind events in a coupled general circulation model. *Climate Dyn.,* **23,** 601–620.

Liebmann, B., and C. A. Smith, 1996: Description of a complete (interpolated) outgoing longwave radiation dataset. *Bull. Amer. Meteor. Soc.,* **77,** 1275–1277.

Lin, J.-L., 2007: The double-ITCZ problem in IPCC AR4 coupled GCMs: Ocean–atmosphere feedback analysis. *J. Climate,* **20,** 4497–4525.

——, and Coauthors, 2006: Tropical intraseasonal variability in 14 IPCC AR4 climate models. Part I: Convective signals. *J. Climate,* **19,** 2665–2690.

McPhaden, M. J., 1999: Genesis and evolution of the 1997–98 El Niño. *Science,* **283,** 950–954.

——, and X. Yu, 1999: Equatorial wave and the 1997–98 El Niño. *Geophys. Res. Lett.,* **26,** 2961–2964.

Meinen, C. S., and M. J. McPhaden, 2000: Observations of warm water volume changes in the equatorial Pacific and their relationship to El Niño and La Niña. *J. Climate,* **13,** 3551–3559.

O'Brien, J. J., A. J. Busalacchi, and J. Kindle, 1981: Ocean models of El Niño. *Resource Management and Environmental Uncertainty: Lessons from Coastal Upwelling Fisheries,* M. Glantz and D. Thompson, Eds., John Wiley and Sons, 159–212.

Penland, C., and P. Sardeshmukh, 1995: The optimal growth of tropical sea surface temperature anomalies. *J. Climate,* **8,** 1999–2024.

Picaut, J., F. Masia, and Y. du Penhoat, 1997: An advective-reflective conceptual model for the oscillatory nature of the ENSO. *Science,* **277,** 663–666.

Rasmusson, E. M., and T. H. Carpenter, 1982: Variations in tropical sea surface temperature and surface wind fields associated with the Southern Oscillation/El Niño. *Mon. Wea. Rev.,* **110,** 354–384.

Raymond, D. J., and A. M. Blyth, 1986: A stochastic mixing model for non-precipitating cumulus clouds. *J. Atmos. Sci.,* **43,** 2708–2718.

——, and ——, 1992: Extension of the stochastic mixing model to cumulonimbus clouds. *J. Atmos. Sci.,* **49,** 1968–1983.

Rayner, N. A., D. E. Parker, E. B. Horton, C. K. Folland, L. V. Alexander, D. P. Rowell, E. C. Kent, and A. Kaplan, 2003: Global analyses of sea surface temperature, sea ice, and night marine air temperature since the late nineteenth century. *J. Geophys. Res.,* **108,** 4407, doi:10.1029/2002JD002670.

Richter, J. H., and P. J. Rasch, 2008: Effects of convective momentum transport on the atmospheric circulation in the Community Atmosphere Model, version 3 (CAM3). *J. Climate,* **21,** 1487–1499.

Schneider, E. K., and R. S. Lindzen, 1976: A discussion of the parameterization of momentum exchange by cumulus convection. *J. Geophys. Res.,* **81,** 3158–3180.

Sherwood, S. C., 1999: Convective precursors and predictability in the tropical western Pacific. *Mon. Wea. Rev.,* **127,** 2977–2991.

Slingo, J. M., and Coauthors, 1996: Intraseasonal oscillations in 15 atmospheric general circulation models: Results from an AMIP diagnostic subproject. *Climate Dyn.,* **12,** 325–357.

Song, X. L., X. Q. Wu, G. J. Guang, and R. Arritt, 2008: Dynamical effects of convective momentum transports on global climate simulations. *J. Climate,* **21,** 180–194.

Suarez, M. J., and P. S. Schopf, 1988: A delayed action oscillator for ENSO. *J. Atmos. Sci.,* **45,** 3283–3287.

Taylor, K. E., 2001: Summarizing multiple aspects of model performance in a single diagram. *J. Geophys. Res.,* **106,** 7183–7192.

Vecchi, G. A., 2006: The termination of the 1997–98 El Niño. Part II: Mechanisms of atmospheric change. *J. Climate,* **19,** 2647–2664.

——, and D. E. Harrison, 2000: Tropical Pacific SST anomalies, El Niño and equatorial westerly wind events. *J. Climate,* **13,** 1814–1830.

Wang, C., 2001: A unified oscillator model of the El Niño–Southern Oscillation. *J. Climate,* **14,** 98–115.

——, and J. Picault, 2004: Understanding ENSO physics—A review. *Earth's Climate: The Ocean-Atmosphere Interaction,* C. Wang, S.-P. Xie, and J. A. Carton, Eds., Amer. Geophys. Union, 21–48.

Wheeler, M., and G. N. Kiladis, 1999: Convectively coupled equatorial waves: Analysis of clouds and temperature in the wavenumber–frequency domain. *J. Atmos. Sci.,* **56,** 374–399.

Wittenberg, A. T., A. Rosati, N.-C. Lau, and J. J. Plashay, 2006: GFDL's CM2 global coupled climate models. Part III: Tropical Pacific climate and ENSO. *J. Climate,* **19,** 698–722.

Wyrtki, K., 1975: El Niño—The dynamic response of the equatorial Pacific Ocean to atmospheric forcing. *J. Phys. Oceanogr.,* **5,** 572–584.

Yu, L., R. A. Weller, and W. T. Liu, 2003: Case analysis of a role of ENSO in regulating the generation of westerly wind bursts in the Western Equatorial Pacific. *J. Geophys. Res.,* **108,** 3128, doi:10.1029/2002JC001498.

Zavala-Garay, J., C. Zhang, A. M. Moore, and R. Kleeman, 2005: The linear response of ENSO to the Madden–Julian oscillation. *J. Climate,* **18,** 2441–2459.

Zhang, C., and J. Gottschalck, 2002: SST anomalies of ENSO and the Madden–Julian oscillation in the equatorial Pacific. *J. Climate,* **15,** 2429–2445.

Zhang, G. J., and N. A. McFarlane, 1995: Sensitivity of climate simulations to the parameterization of cumulus convection in the Canadian Climate Centre general circulation model. *Atmos.–Ocean,* **33,** 407–446.